

SHUTTLE ACTIVE THERMAL CONTROL SYSTEM
DEVELOPMENT TESTING

VOLUME VI
WATER EJECTOR PLUME TESTS

Report No. T169-28

16 November 1973

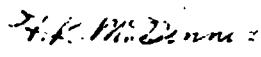
Submitted By

VOUGHT SYSTEMS DIVISION
LTV Aerospace Corporation
Dallas, Texas

To

THE NATIONAL AERONAUTICS AND SPACE ADMINISTRATION
Lyndon B. Johnson Space Center
Houston, Texas

Prepared by:


F. K. McGinnis


R. M. Summerhays

Approved by.


R. J. French, Supervisor
EC/LS Group

FOREWORD

This volume is one of a series of reports describing the development tests conducted on a candidate Shuttle heat rejection system at the National Aeronautics and Space Administration - Johnson Space Center during the period from March to July 1973. The complete test series are reported in the following volumes:

- Volume I Overall Summary
- Volume II Modular Radiator System Tests
- Volume III Modular Radiator System Test Data
Correlation With Thermal Model
- Volume IV Modular Radiator System Test Data
- Volume V Integrated Radiator/Expendable Cooling System
Tests
- Volume VI Water Ejector Plume Tests
- Volume VII Improved Radiator Coating Adhesives Tests
- Volume VIII Tube Anomaly Investigation

The tests were conducted jointly by NASA and the Vought Systems Division of LTV Aerospace Corporation under Contract NAS9-70534. D. W. Morris of the NASA-JSC Crew Systems Division was the contract technical monitor. Mr. R. J. Tufte served as the VSD Project Engineer.

TABLE OF CONTENTS

		<u>PAGE</u>
1.0	INTRODUCTION AND SUMMARY	1
2.0	TEST ARTICLES, INSTRUMENTATION, AND PROCEDURE	4
3.0	RESULTS AND DISCUSSION	7
	3.1 Test Conditions	7
	3.2 Baratron and Ion Gage Data	7
	3.3 QCM Data	10
4.0	CONCLUSIONS	16
5.0	REFERENCES	17

APPENDICES

A	FLASH EVAPORATOR AND SUBLIMATOR EXHAUST PLUME FLOW FIELD PREDICTIONS	A-1
---	---	-----

LIST OF FIGURES

		<u>PAGE</u>
1	Plugged Nozzle Configuration	18
2	Locations of Plume Measurement Devices	19
3	Phase III Test Setup Chamber A	20
4	Phase IIIA Test Setup In Chamber A	21
5	Impact Pressure Data - Evaporator With No Nozzle	22
6	Impact Pressure Data - Sublimator With Supersonic Nozzle	23
7	Impact Pressure Data - Sublimator With Supersonic Nozzle	24
8	Impact Pressure Data - Evaporator with Plugged Nozzle.	25
9	Impact Pressure Data - Evaporator with Plugged Nozzle.	26
10	Impact Pressure Data - Supersonic Nozzle - Ion Gage #7	27
11	Impact Pressure Data - No Nozzle - Ion Gage #7	28
12	Impact Pressure Data - Supersonic Nozzle-Ion Gage #3	29
13	Impact Pressure Data - Supersonic Nozzle-Ion Gage #1	30
14	Mass Flux Data - Supersonic Nozzle - QCM #4.	31
15	Mass Flux Data - No Nozzle - QCM #4	32
16	Mass Flux Data - Phase III Test - QCM #9	33
17	Mass Flux Data - Phase IIIA Test - QCM #8	34
18	Mass Flux Data - Phase IIIA Test - QCM #9	35
19	Effect of Expansion Angle on Plume Back Flow	36

1.0 INTRODUCTION AND SUMMARY

This report presents the results of vacuum testing of nozzles designed to eject water vapor away from the Space Shuttle to prevent contamination of the spacecraft surfaces and payload. The water vapor is generated by an active cooling system which evaporates excess fuel cell water to supplement a Modular Radiator System (MRS). The complete heat rejection system including the MRS, flash evaporator or sublimator and nozzle were first tested to demonstrate the system operational characteristics. This data is presented in Volume V of this report, "Integrated Radiator/Evaporator Tests". No plume data were obtained from that test. The data presented in this report are from a test which included only the flash evaporator or sublimator and nozzles. The MRS was not included in this test but the active devices were operated in the same manner as observed in the system tests.

The plume tests were performed in two phases in the Space Environment Simulation Laboratory (SESL) Chamber A at NASA/JSC. The first tests, designated Phase III, were conducted from June 11 through June 14, 1973 and included a supersonic nozzle and a sonic nozzle (orifice). A plugged nozzle was tested in the second test, Phase IIIA, on July 16 and 17, 1973. The objectives of this test series were as follows:

- o To determine the effectiveness of a supersonic nozzle and a plugged nozzle in minimizing impingement upon the spacecraft of water vapor exhausted by an active device (flash evaporator or sublimator)
- o To obtain basic data on the flow fields of exhaust plumes generated by these active devices, both with and without nozzles installed.

The nozzles were designed and fabricated by the Propulsion and Power Division (PPD) of JSC, which also had primary responsibility for test definition and instrumentation selection and location within the chamber. Yought Systems Division (VSD) of LTV Aerospace Corporation provided and operated the flash evaporator and the flow bench which supplied the heat load for the active devices. Hamilton Standard Division (HSD) of United Aircraft Corporation provided the sublimator. In addition to the operation of the flow bench and flash evaporator, VSD was tasked to provide support of plume test definition and the tests themselves, plus an assessment of the results. In this role, VSD put forth recommendations in the area of plume instrumentation and provided real time test support and data reduction. This report constitutes the VSD evaluation of the significant results of the tests.

In summary, the MRS Phase III Plume Test results lead to the following conclusions:

- o Predicted and measured flow field properties (impact pressure and mass flux) are in reasonable agreement for both the supersonic nozzle and sonic orifice (no nozzle) configurations. Measured plume properties for the plugged nozzle indicate that the flow field can be modeled analytically as a sonic orifice with reduced nozzle exit expansion angles.
- o Because of inadequate data from the backflow instrumentation during the Phase III test, the accuracy of the analytical models could not be verified for large plume expansion angles. As a result, the effectiveness of the supersonic nozzle relative to the no nozzle

configuration in reducing impingement on the spacecraft surface could not be completely resolved. However, the available data, coupled with the substantiation of the prediction techniques for the supersonic nozzle in the Phase IIIA tests, tend to confirm previous predictions (Reference 1) that the supersonic nozzle will reduce impingement by a factor of approximately three to ten. Phase IIIA data indicate that the plugged nozzle provides a reduction in impingement by a factor of 25 to 100 relative to the no nozzle configuration.

- o The test data also indicate that intermittent or pulsing operation, as in the case of the flash evaporator, and steady flow operation, as in the case of the sublimator, do not differ significantly from the standpoint of plume impingement, for the same time-average mass flowrate.

2.0 TEST ARTICLES, INSTRUMENTATION, AND PROCEDURE

The test articles consisted of a VSD flash evaporator and a HSD sublimator, both capable of operating at a nominal 16 lb/hr water flow rate. These devices were equipped with exhaust ducts approximately six feet in length and containing two 45° bends. Provision was made for mounting nozzles on the duct ends. For the sonic flow test conditions, the sublimator exhausted directly from the duct, while the flash evaporator exhausted through a calibrated converging nozzle. For the supersonic nozzle tests, NASA-JSC designed and fabricated heated, contoured nozzles with the following characteristics:

Device	Nozzle Properties				
	Expansion Ratio	Length	Throat Dia.	Exit Dia.	Exit Angle
Flash Evaporator	10	12.8"	2.18"	6.90"	7.33°
Sublimator	10	30.8"	6.15"	19.45"	6.89°

Figure 1 shows a schematic of the plugged nozzle which was tested with the flash evaporator in the Phase IIIA tests. The nozzle exit area is annular with an outside diameter equal to that for the supersonic nozzle (6.90 inches) but with an effective area equal to that for the sonic orifice. The nozzle design, with the indicated exit angle of approximately 67 degrees at the outer diameter, is intended to direct flow toward the centerline and reduce plume expansion angle.

The types, locations, and identifying numbers for the various pieces of plume instrumentation for the Phase III tests are shown in Figure 2. Figure 3 is a schematic showing these locations relative to the test

chamber. For the Phase IIIA tests several changes were made on the basis of data problems which occurred in Phase III. Specifically, the more distant Baratron gages (#2, #6, and #7) were moved closer to the nozzle exit and the orientation of the QCM's in the nozzle exit plane (#7, #8, and #9) was changed. The Phase IIIA instrumentation locations and orientations are shown in Figure 4.

Baratron gages with pitot-tube-like tubulations were used for impact pressure measurements in the plume near field, while ion gages were employed in the more distant regions. Quartz crystal microbalances (QCM's) were used in parallel with the ion gages and were also located in the nozzle exit plane in order to measure "back-flow". These devices must be cryogenically cooled for purposes of mass collection and their natural frequency increases as mass accumulates until a saturation point is reached. Thus the QCM's have a finite operating time, after which they must be dried out and recooled before they are again usable. Particle spectrometers supplied by NASA-MSFC were the final type of instrumentation used. These devices are capable of measuring particulate matter over the size range from 0.1 to 420 microns. However, these devices did not operate properly during either test and no significant data were obtained.

In the actual test procedure, the device to be tested (flash evaporator or sublimator) was translated into the position shown in Figure 2, relative to the instrumentation. After establishing the desired device operating condition and cooling down the QCM's, plume data were taken in several forms. First direct readings of the Baratron and ion gage outputs were made. Data from these sensors were also recorded on strip charts and on the ACE data system, as a function of time. Second, QCM outputs were recorded and plotted manually as a function of time. As soon as sufficient QCM data were obtained to establish a linear variation of QCM output with

time (corresponding to a constant mass flux), the test point was declared complete. This procedure greatly expedited testing by minimizing the mass accumulation on the QCM's at each test point and hence minimizing the frequency of time consuming QCM warm-up/cool-down procedures.

3.0 RESULTS AND DISCUSSION

Representative test results are summarized in this section, compared with predictions where applicable, and evaluated as to their significance.

3.1 Test Conditions

The actual test conditions achieved are summarized as follows, where the device/condition order corresponds to the actual test sequence:

<u>Test</u>	<u>Device/Condition</u>	<u>Average Water Flow Rates (lb/hr)</u>
III	Sublimator with supersonic nozzle	3.5, 7.3, 13
III	Flash Evaporator with supersonic nozzle	2, 4, 8, 16
III	Sublimator without nozzle	2.1, 4.2, 9.1, 17.1
III	Flash Evaporator without nozzle	1.7, 3.1, 5.3, 8.0, 16.0
IIIA	Sublimator with supersonic nozzle	2.7, 8.4, 15.7
IIIA	Flash Evaporator with plugged nozzle	1.9, 7.4, 16.0

It should be noted here that the flash evaporator and sublimator do function in distinctly different control modes. The flash evaporator is designed for a single flow rate conditions (16 lb/hr) and is pulse modulated to achieve lower average flow rates. Therefore, instantaneous plume flow field properties, such as impact pressure always correspond to the single flow rate of 16 lb/hr. Long-term properties, such as accumulation of mass on the QCM's, reflect the average flow rate. In the case of the sublimator, the flow rate is continuously variable, so that both instantaneous and long-term properties reflect the average flow rate indicated in the table above.

3.2 Baratron and Ion Gage Data

Some difficulty was encountered in establishing and maintaining the zeros on the Baratron gages. This fact, coupled with the failure of several

Baratron heads, resulted in there being usable data from only two of these devices, #1 and #4, during the Phase III test. For the Phase IIIA test, as noted previously, three of the gages were moved closer to the nozzle to obtain higher readings relative to background, and usable data was obtained on all seven of the Baratrons during portions of this test. The ion gages generally performed well throughout both tests, but also suffered somewhat from zeroing problems and marginal signal-to-noise ratio at the distant locations.

Typical Baratron and ion gage data are shown in Figures 5 through 9 as a function of location in the plume flow field. The specific test conditions correspond to the flash evaporator without a nozzle (Figure 5), the sublimator with supersonic nozzle (Figures 6 and 7), and the flash evaporator with plugged nozzle (Figures 8 and 9). The coordinate system is nozzle-based, with the origin at the exit plane, and gage readings are indicated in millimeters of mercury. For the low density plumes in these tests the readings should be representative of impact pressure. Impact pressure predictions have been made using techniques which are described in Reference 2 and summarized in Appendix A of this report, and these predictions, in the form of lines of constant impact pressure, are also shown in Figures 5 through 9. The predicted values for the no nozzle and supersonic nozzle cases are based on actual pretest predictions, with the effects of nozzle boundary layer included in the supersonic nozzle case. For the plugged nozzle, as discussed in Appendix A, the impact pressure predictions represent a fit of the data to a modified sonic orifice plume distribution.

The measurements are seen to be in general agreement with the predictions. It is apparent from Figures 5 and 6 that the supersonic nozzle configuration resulted (as predicted) in generally higher impact pressure

readings than for the configuration with no nozzle, reflecting its tendency to concentrate mass flow near the centerline. A similar trend is apparent from Figures 5 and 8, with plugged nozzle giving consistently higher impact pressure readings at the ion gage locations between the centerline and 40-degrees. A comparison of the supersonic nozzle and plugged nozzle flow fields can best be made from the baratron data in Figures 7 and 9. The supersonic nozzle appears to concentrate more flow near the centerline (at angles less than approximately 30 degrees), but the plugged nozzle gives higher readings at the gages (#5 and #7) at angles greater than 30 degrees. This indicates the plugged nozzle gives a flatter profile near the centerline which, in conjunction with the close agreement with the predicted lines in Figures 8 and 9 tends to confirm the assumption that the plugged nozzle flow field can be adequately represented by a modified sonic orifice distribution.

Figures 10 through 13 show data for impact pressure measured by the ion gages as a function of flow rate. As noted in Section 3.1, the 16 lb/hr data for the flash evaporator uniquely define the impact pressure properties of its plume field. However, the sublimator plume does undergo changes in impact pressure levels as the flow is varied, and provided test data as a function of flow rate. Figure 10 shows data for the supersonic nozzle in the Phase IIIA test at ion gage #7, which is located at the largest angle (40 degrees) from the plume centerline. Also shown is the predicted pressure variation, based on the analysis in Appendix A. Some non-linearity in the test data is observable, but in general there is good correlation with the predictions, particularly, at the lower flow rates. Ion gage #7 data for the no nozzle case are shown in Figure 11, and also show good correlation with the analytic predictions. Figures 12 and 13 show supersonic nozzle data for ion gages #3 and #1 respectively, which represent

the measurements closest to the plume centerline and at an intermediate angle of 24 degrees. The close correlation with prediction in Figures 10 through 13 tends to further confirm the adequacy of the prediction techniques for angles up to 40 degrees.

3.3 QCM Data

As a result of installation damage to some devices and the inability to maintain adequate cryogen flow to those near the tcp of the chamber, only a limited number of QCM's were operational during the tests. QCM's #4 and #9 operated reliably during the Phase III tests, while QCM's #4, #8, and #9 were operational for Phase IIIA. The data from QCM's #8 and #9 are of particular importance because these devices were located in the nozzle exit plane and were the only instruments available for correlating backflow of the plumes. The QCM's were also the only devices providing data on the flash evaporator during low flow or pulsing operation.

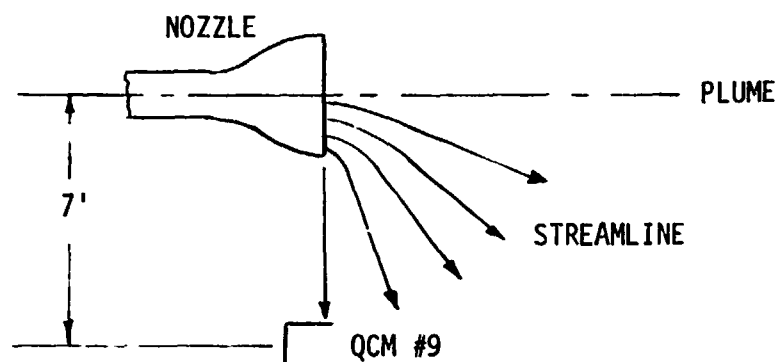
Impingement mass flux data obtained with QCM #4 during the Phase III tests are shown in Figure 14 for the supersonic nozzle and Figure 15 for the no nozzle configuration, as a function of device average flow rate. These plots differ from the impact pressure presentation in that the long-term nature of the QCM measurements provided flash evaporator data points corresponding to time-average flow rates less than the maximum of 16 lb/hr, permitting the sublimator and flash evaporator data to be plotted together on the same graph. For the pulsing condition the QCM outputs were observed to change slope slightly during the device operation portion of the duty cycle, but the basic time-average linear variation was apparent.

In the Phase III test configuration QCM #4 was apparently partially blocked by a baratron strut. The fact that the QCM #4 data, as shown in Figures 14 and 15, were consistently lower, by approximately a factor of two,

than the predicted values is attributed to this blockage. Data from the sublimator test with the supersonic nozzle from the Phase IIIA test, where the blockage did not exist, have also been plotted in Figure 14 for reference, and show relatively good correlation with prediction.

The interesting feature of Figures 14 and 15 is the fact that the sublimator and flash evaporator data do lie along the same straight line. Hence the two devices, which operate in radically different fashion, would appear to have the same potential for spacecraft contamination under given mass flow rate (heat load) conditions. The sublimator contamination potential increases with flow rate by virtue of increasing the plume density at any point, while the flash evaporator contamination increases in the same proportion by virtue of an increasing frequency of 16 lb/hr pulses. There is no evidence that plume growth/collapse phenomena associated with pulsing operation significantly affect the contamination potential of the flash evaporator plume. It is also interesting to note that the measured plume properties do not differ significantly between the nozzle/no nozzle cases at the moderate off-axis position of QCM #4, which is in agreement with predictions.

The orientation of QCM #9 in the Phase III test makes it difficult if not impossible to predict what that QCM should have measured. This situation is explained with the aid of the following sketch:



At radial distances a few feet from the nozzle exit, the plume flow streamlines (Molecule paths) tend to be radial, with their origin at the nozzle exit. With QCM #9 oriented as illustrated, its collecting aperture was 90° to the local flow direction and hence presented a very small capture area for plume molecules. The actual effective value of this capture area is unknown.

However, since the Phase III test provides the only data for backflow with the no nozzle configuration, the QCM #9 data have been used to compare measured and predicted supersonic nozzle effectiveness on a relative basis: that is, on the basis of the ratio of QCM #9 mass fluxes with and without the nozzle. These data are presented in Figure 16 as a function of device flow rate. The data are scattered, particularly for the no nozzle case, but the general trends are as expected: the supersonic nozzle configuration resulted in less backflow than with no nozzle and the backflow tended to increase with increasing flow rate. The estimated means for the data from the two configurations shows a reduction of approximately a factor of three with the supersonic nozzle, compared with a predicted value of 3.7 from the analysis in Appendix A.

The reorientation of the backflow QCM's in the Phase IIIA tests resulted in much more significant data from both QCM #8 and QCM #9, and permitted a direct correlation between the supersonic and plugged nozzles. These data are shown in Figures 17 and 18 as a function of device flow rate, with analytic predictions also presented.

Several trends can be observed from the data in Figures 17 and 18. One factor is that the supersonic nozzle gave consistently lower readings than predicted, particularly for QCM #8 where the variation was almost a

factor of two. The low readings at QCM #8 may be partially explainable by the relatively short distance (4 feet) between the QCM and the nozzle centerline, which gives an r/r^* ratio of approximately 15 to 1 for the supersonic nozzle. The plume may not be fully expanded, or the flow radial, at this location. The trend of all the data indicates, however, that the supersonic nozzle may be somewhat more effective at reducing backflow than predicted.

For the plugged nozzle both QCM #8 and QCM #9 data show a trend toward somewhat higher readings relative to prediction at the lower flow rates. Since the plugged nozzle was used with the flash evaporator, this trend could indicate that some effect on plume distribution from the buildup and collapse of the plume during pulsing operation of the evaporator is observable at the 90-degree location. However, the data is considered inconclusive, particularly since a similar trend was not observed for QCM #4 (Figure 14).

The most significant conclusion from the data in Figures 17 and 18 is the marked reduction in backflow for the plugged nozzle over the supersonic nozzle. The reduction is a factor of approximately three to four, which compares with improvement obtained with the supersonic nozzle over the no nozzle configuration. The plugged nozzle data also correlates quite well with predictions based on the analysis in Appendix A. This tends to confirm the assumption that the plugged nozzle flow field can be adequately modeled by a modified sonic orifice distribution.

A more significant parameter than mass flux ratio at 90 degrees for determining nozzle effectiveness is the total mass flow at angles greater than 90 degrees. This parameter must be determined analytically, and the methodology and specific values for each of the three nozzle configurations

in terms of fraction of total flow expanding to angles greater than 90 degrees are presented in Appendix A. This fraction is much more sensitive to small variations in the analytical equations than mass flux values at specific locations. On the basis of the test data it does not appear feasible to establish a single value but rather a range of values for nozzle effectiveness in reducing plume backflow or impingement. This is particularly true for the plugged nozzle, for which a semi-empirical approach was used, as illustrated in Figure 19. This curve shows percent of flow expanding to angles greater than 90 degrees for a sonic orifice as a function of maximum plume expansion angle. The specific values for the plugged nozzle and no nozzle configurations are shown, indicating a reduction of approximately a factor of 60 for the plugged nozzle. However, although the assumed angle of 113 degrees for the plugged nozzle provides the best fit for all the test data, QCM #8 and #9 data indicate a possible range of 110 to 118 degrees, or an effectiveness ratio of 25 to 100.

For the supersonic nozzle there are similar uncertainties due to the sensitivity in defining boundary layer and indications of QCM #8 and #9 data that actual mass flows are somewhat lower than predicted. These data indicate the supersonic nozzle will reduce backflow by a factor of 3 to 10 for the sublimator, with a slightly higher value possible for the flash evaporator because of reduced boundary layer effects with the shorter nozzle.

Caution should be exercised in using the absolute values for fraction of mass flow expanding to angles greater than 90 degrees as a measure of true impingement mass. The test data were obtained in a configuration where no significant amount of structure was present to interfere with plume development. For the case of impingement on a spacecraft surface,

the surface itself will affect the plume distribution in the highly expanded regions and consequently affect the total plume impingement.

4.0 CONCLUSIONS

Based on this analysis of the data from the MRS Phase III and Phase IIIA Plume tests, the following conclusions are drawn:

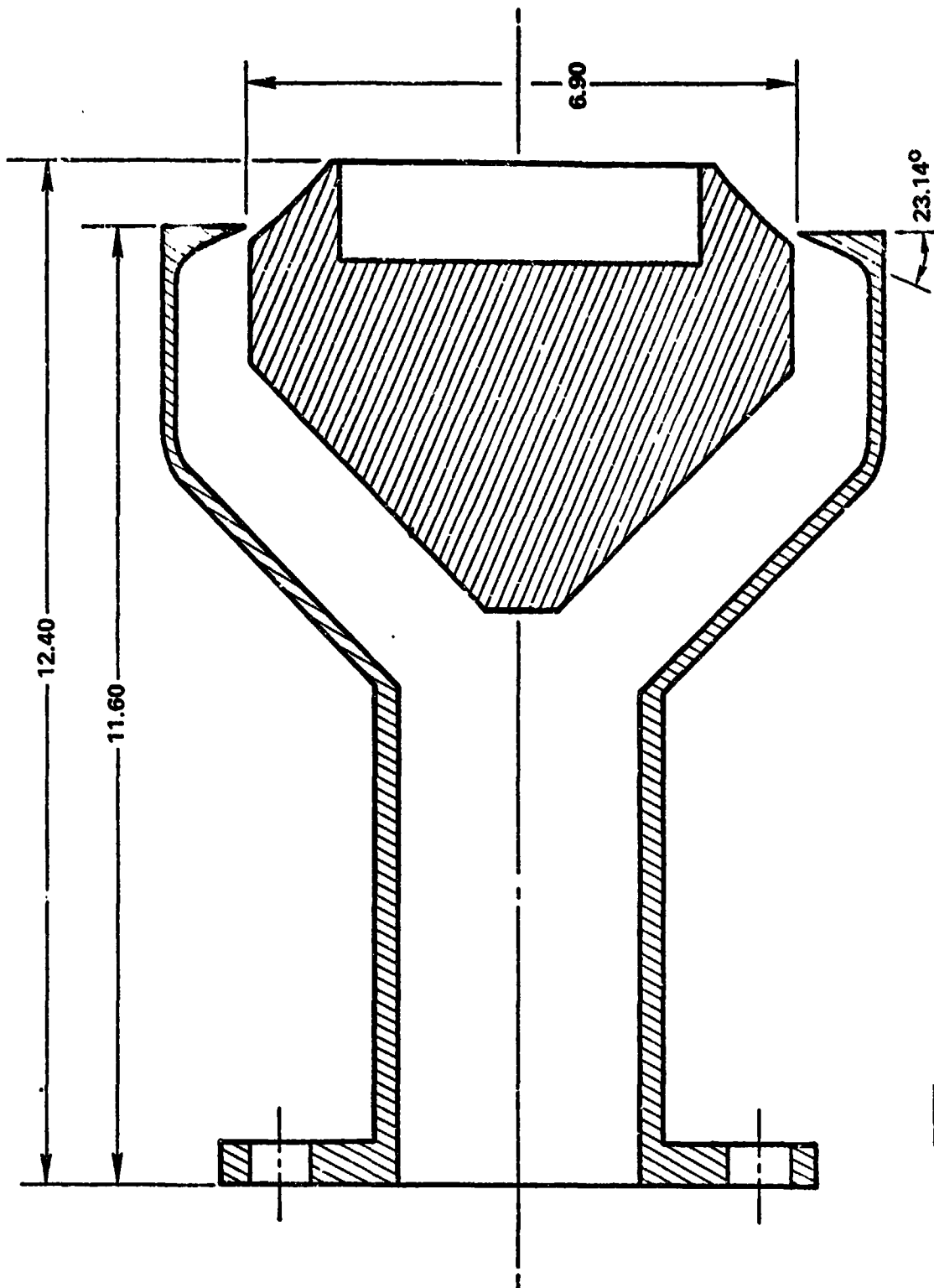
- Flow field property predictions and measurements are in substantial agreement for both the supersonic nozzle and sonic orifice (no nozzle) configurations.
- Test measurements indicate that the plugged nozzle flow field can be adequately modeled by a modified sonic orifice distribution.
- Substantiation of the prediction techniques for the supersonic nozzle and sonic orifice, coupled with backflow sensor data on the supersonic nozzle in the Phase IIIA tests, shows the supersonic nozzle reduces impingement by a factor of three to ten.
- Correlation of the plugged nozzle flow field test data with a modified sonic orifice distribution shows the plugged nozzle reduces impingement by a factor of 25 to 100.
- The pulsing operation of the flash evaporator and the steady-flow mode of the sublimator do not yield significantly different contamination potential at a given average mass flow rate.

5.0 REFERENCES

1. VSD presentation to NASA-JSC Crew Systems Division Personnel, 2 February 1972.
2. McGinnis, F. K., "Some Considerations of Flash Evaporator/Sublimator Exhaust Duct and Plume Flows", VSD Informal Memorandum 2-53002/73IM-15, 14 February 1973.

FIGURE 1

PLUGGED NOZZLE CONFIGURATION




 **VOUGHT SYSTEMS DIVISION**
LTV AEROSPACE CORPORATION

FIGURE 2
LOCATIONS OF PLUME MEASUREMENT DEVICES

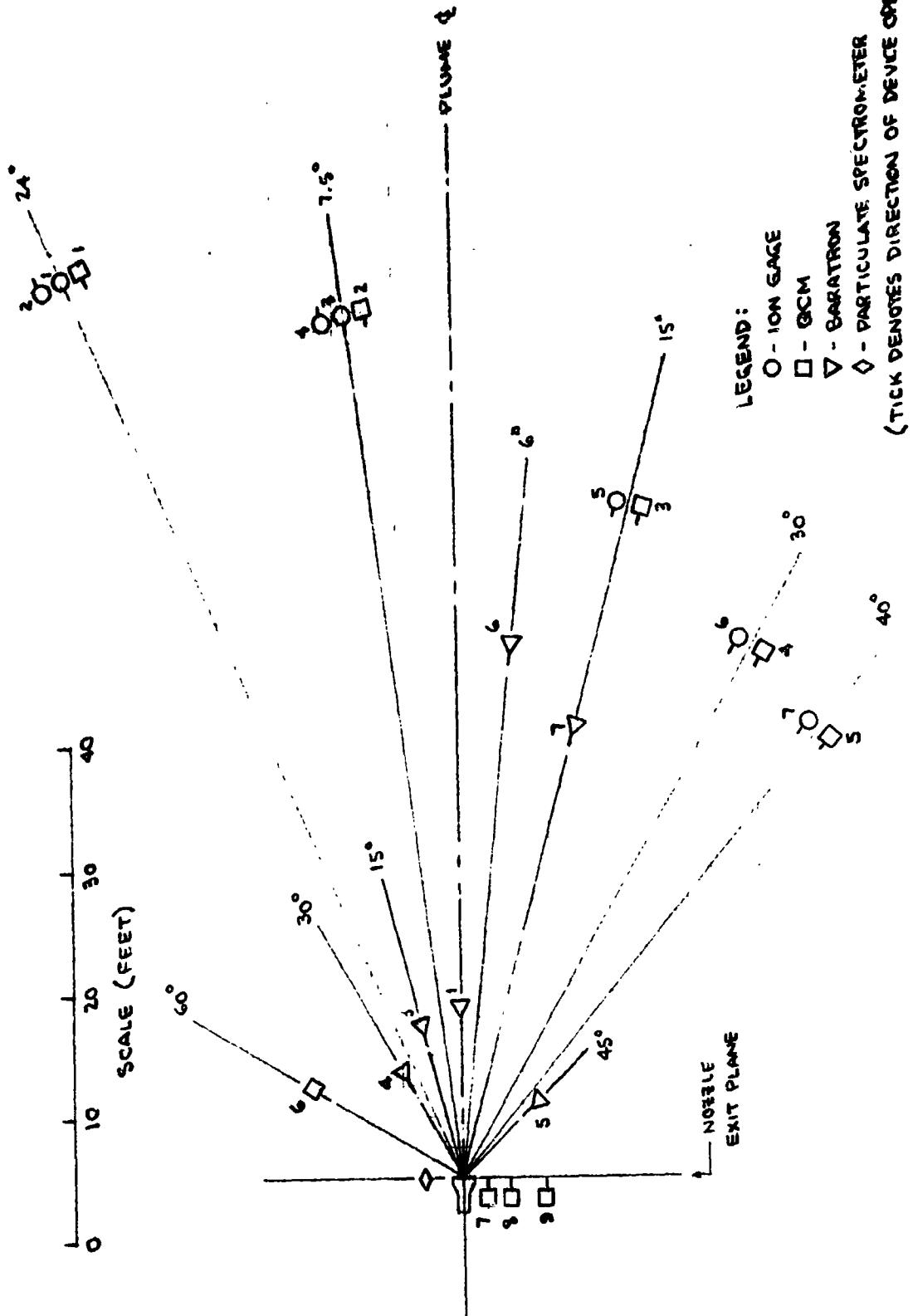


FIGURE 3
PHASE III TEST SETUP CHAMBER A

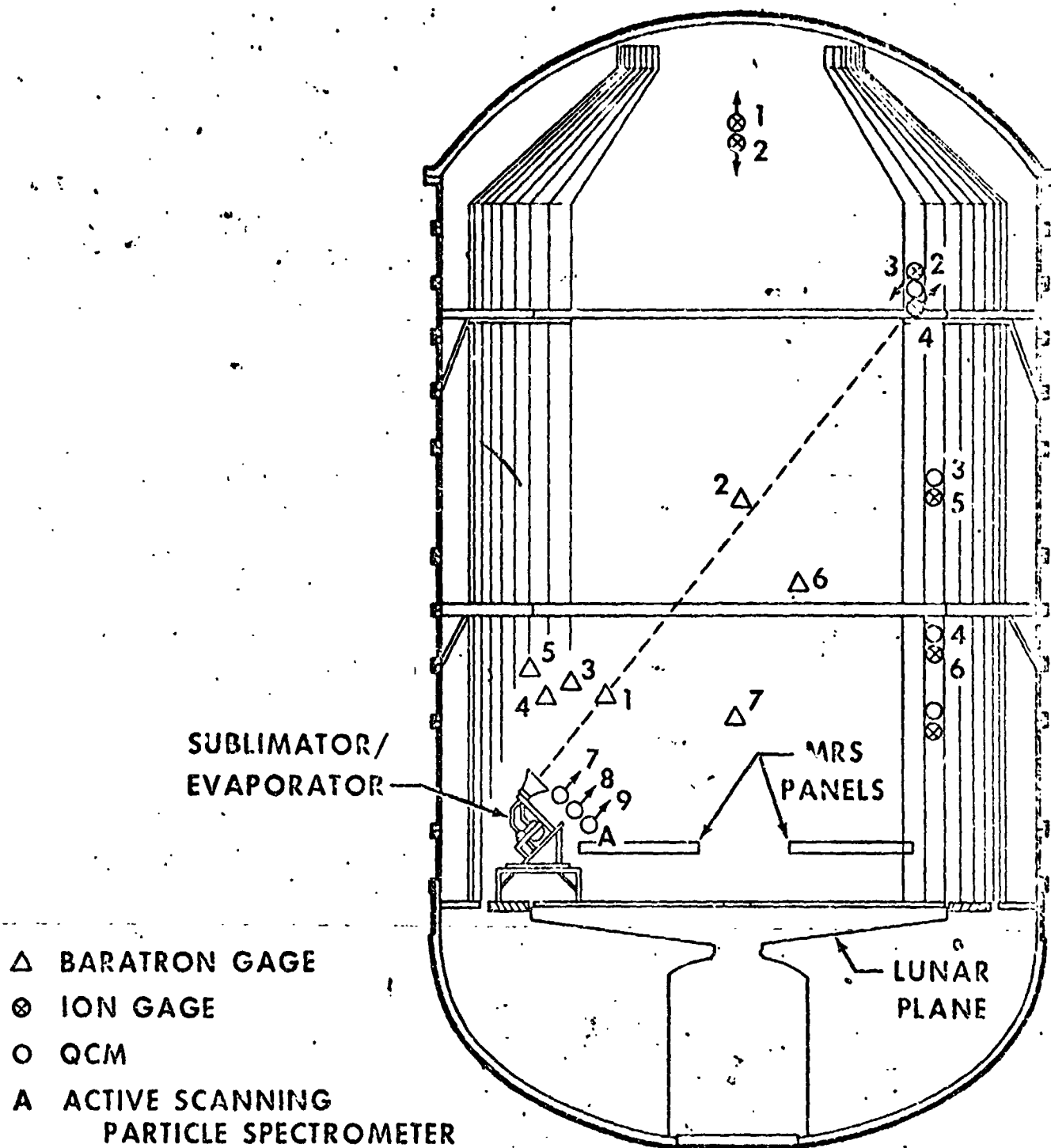


FIGURE 4
PHASE IIIA TEST SETUP IN CHAMBER A

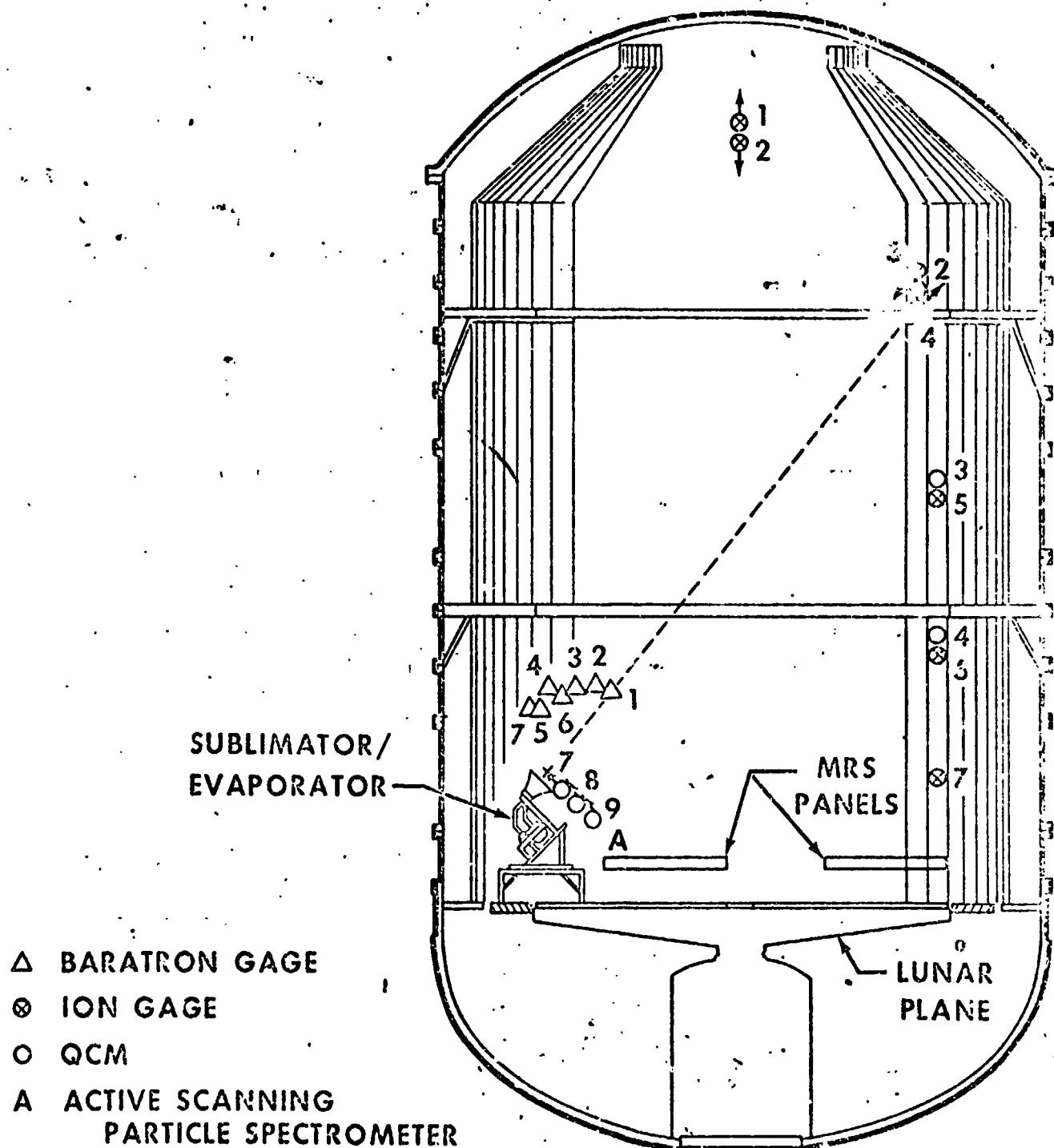


FIGURE 5
IMPACT PRESSURE DATA - EVAPORATOR WITH NO NOZZLE

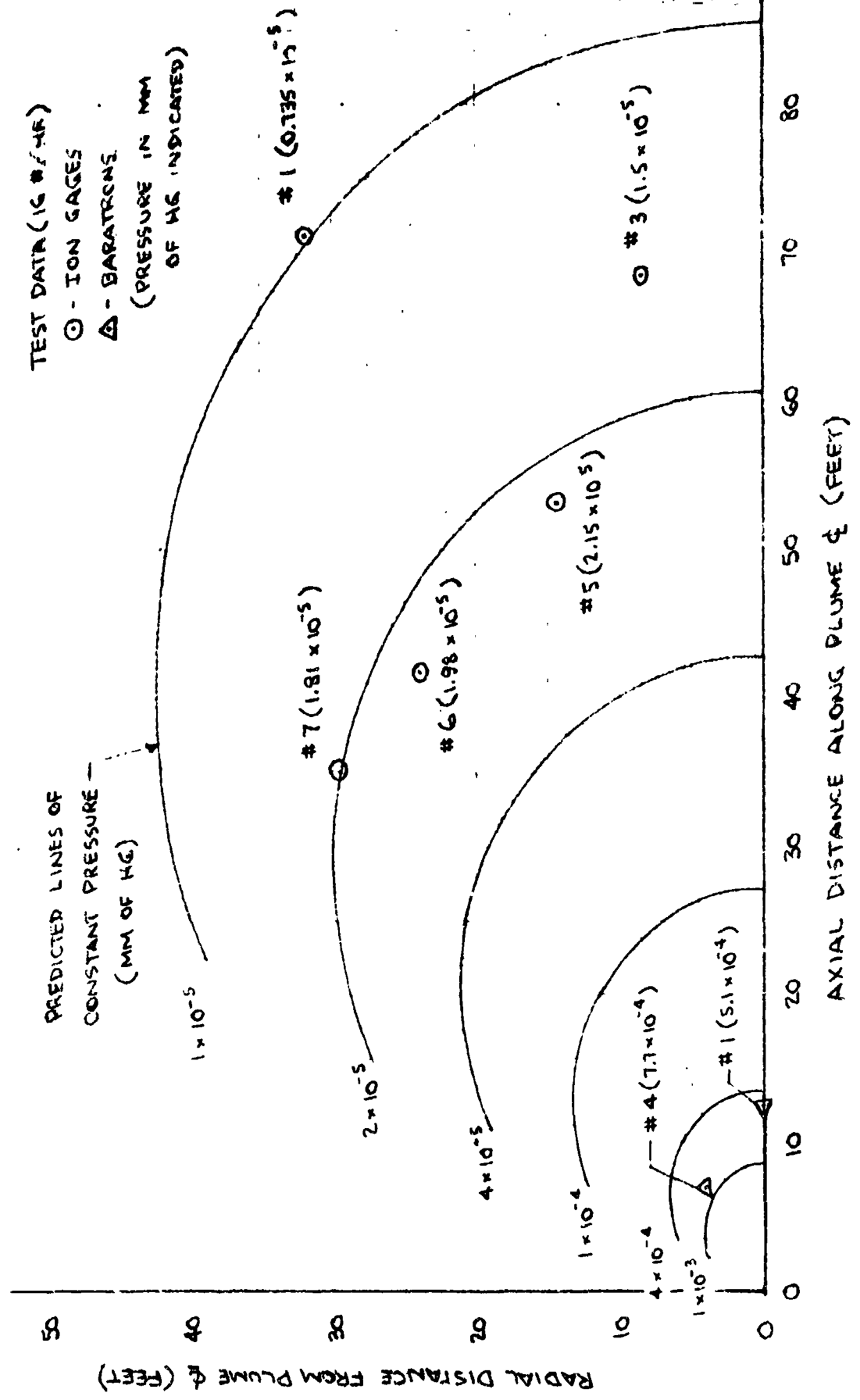


FIGURE 6
IMPACT PRESSURE DATA - SUBLIMATOR WITH SUPERSONIC NOZZLE

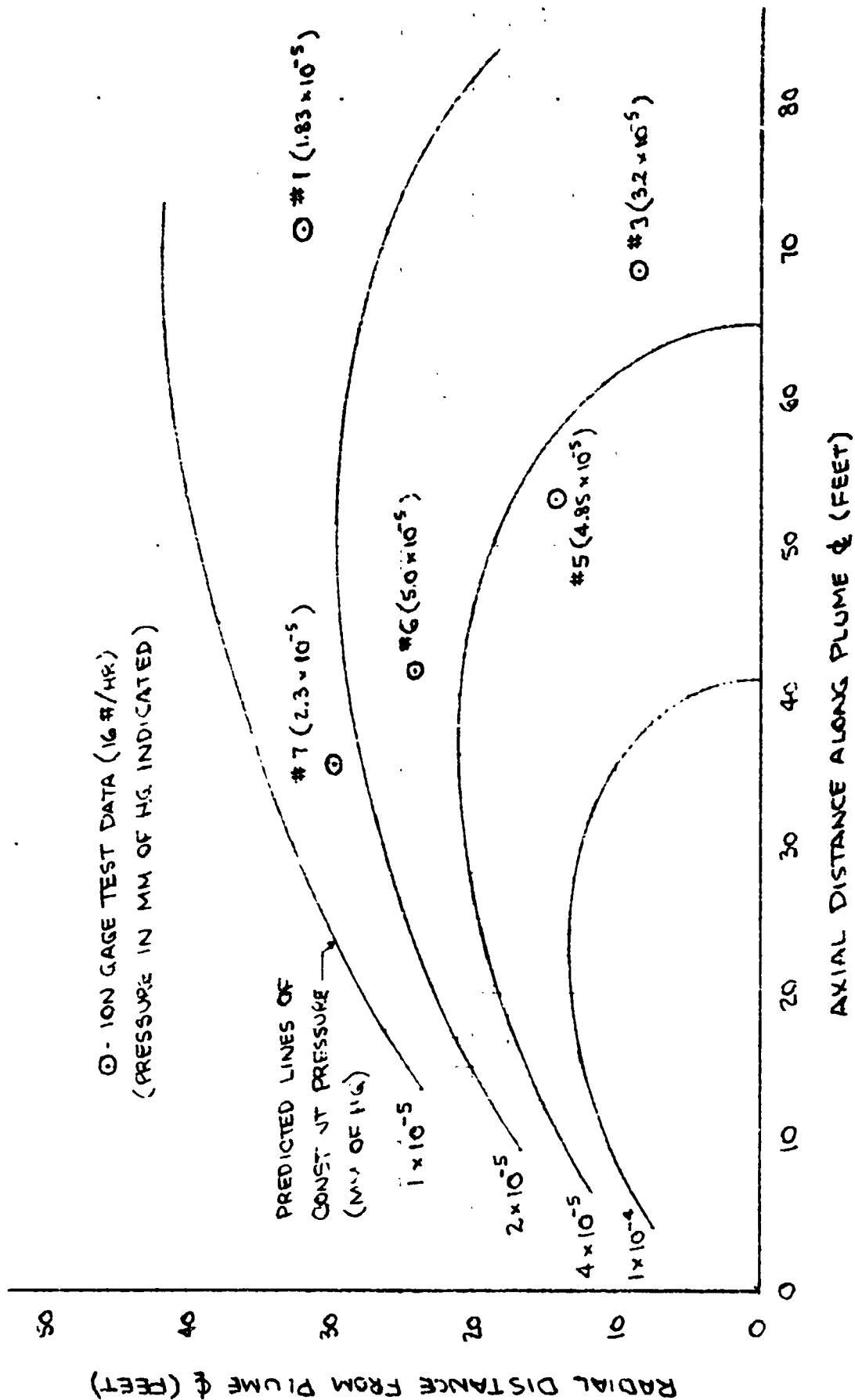


FIGURE 7
IMPACT PRESSURE DATA - SUBLIMATOR WITH SUPERSONIC NOZZLE

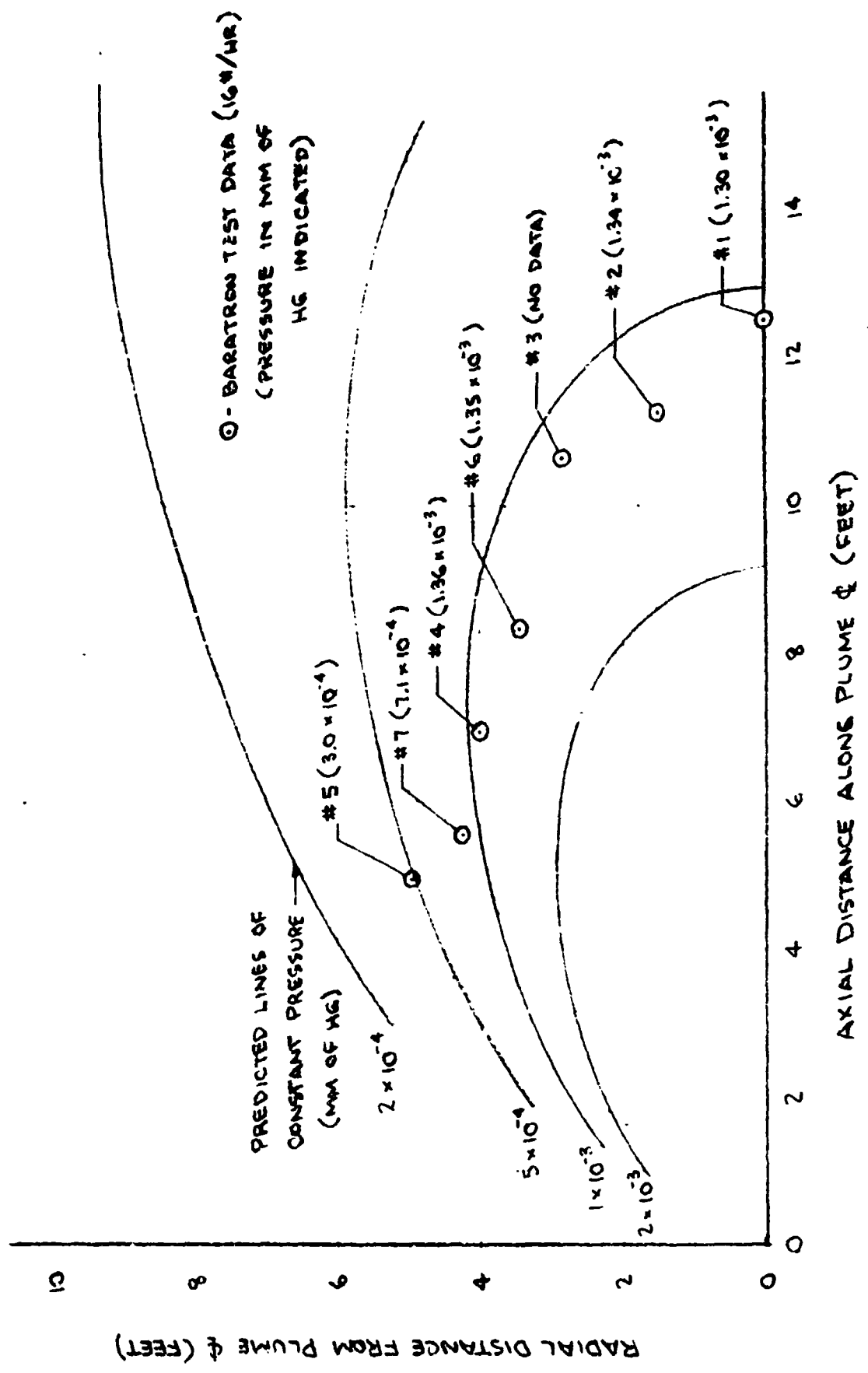


FIGURE 8
IMPACT PRESSURE DATA - EVAPORATOR WITH PLUGGED NOZZLE

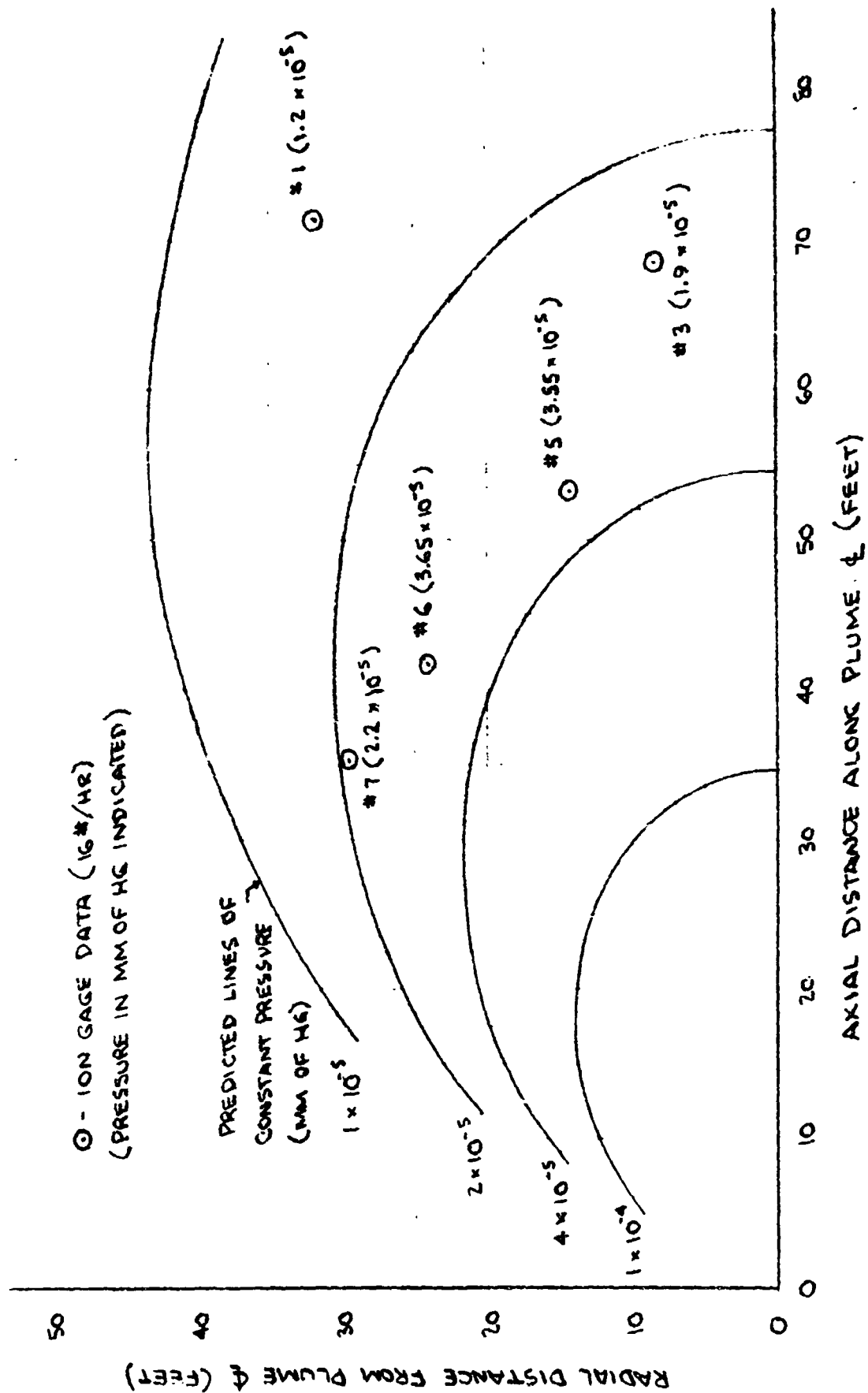


FIGURE 9

IMPACT PRESSURE DATA - EVAPORATOR WITH PLUGGED NOZZLE

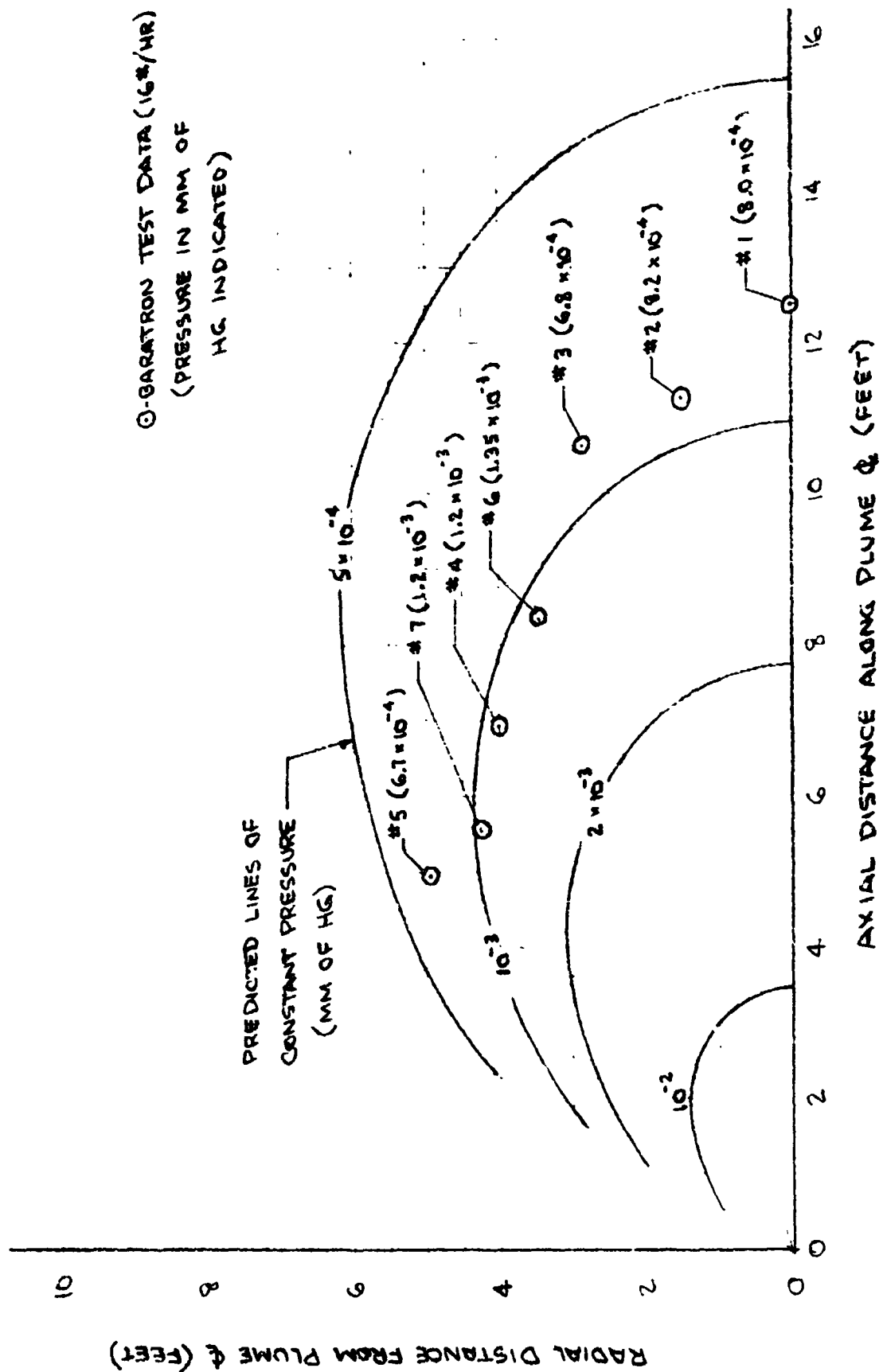


FIGURE 10
 IMPACT PRESSURE DATA - SUPERSONIC NOZZLE - ION GAGE #7

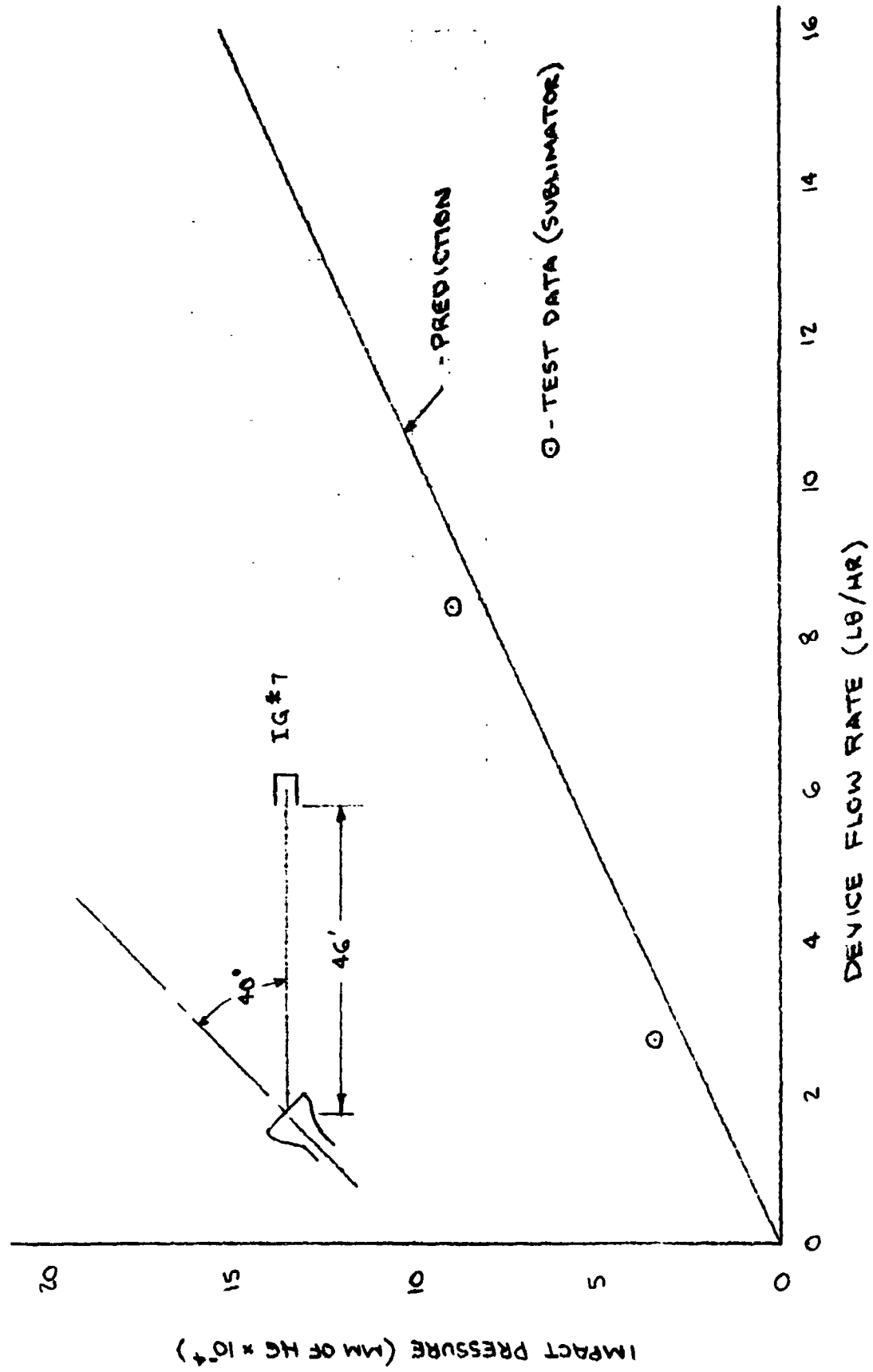


FIGURE 11
IMPACT PRESSURE DATA - NO NOZZLE - ION GAGE #7

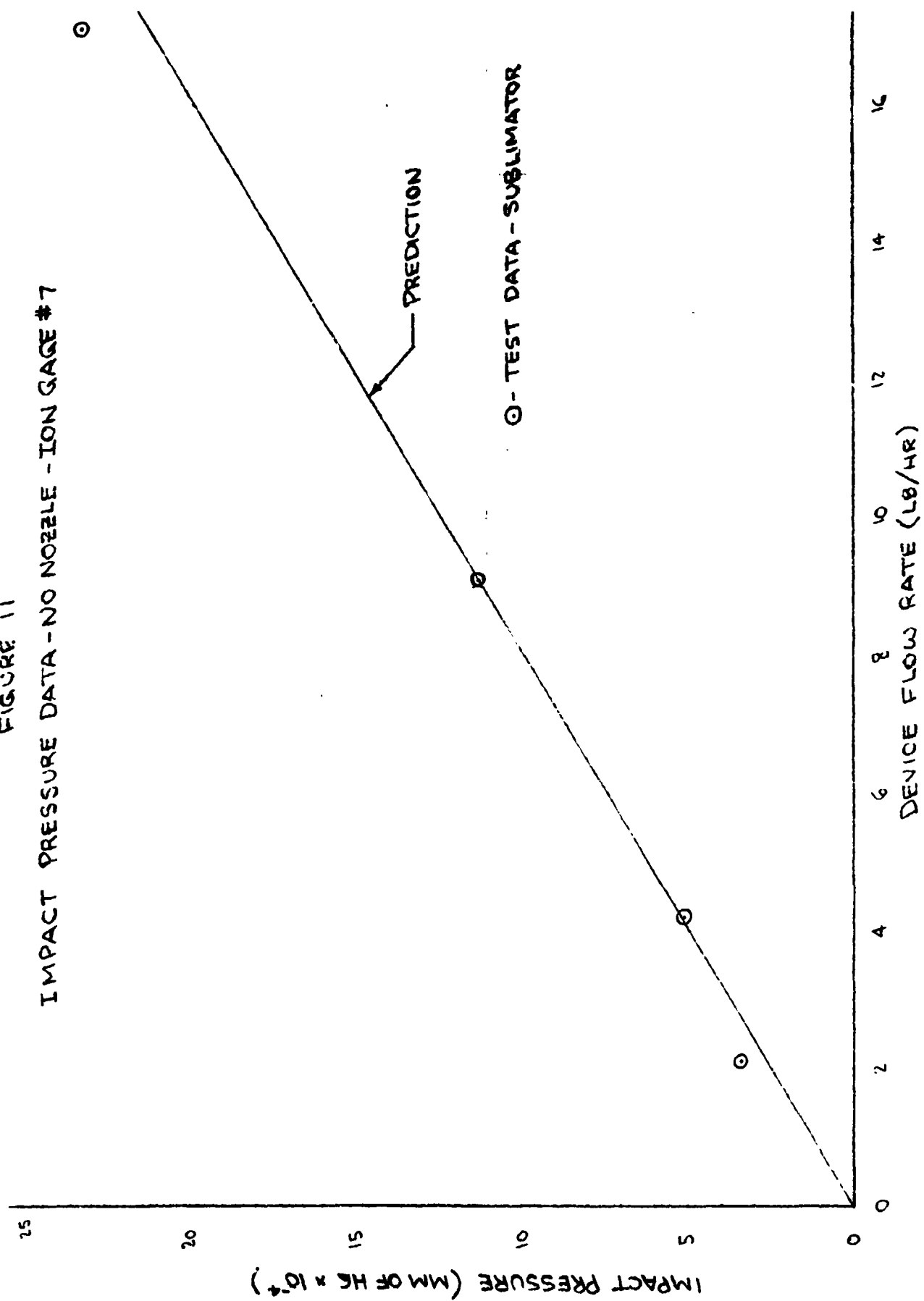


FIGURE 12
IMPACT PRESSURE DATA - SUPERSONIC NOZZLE - ION GAGE #3

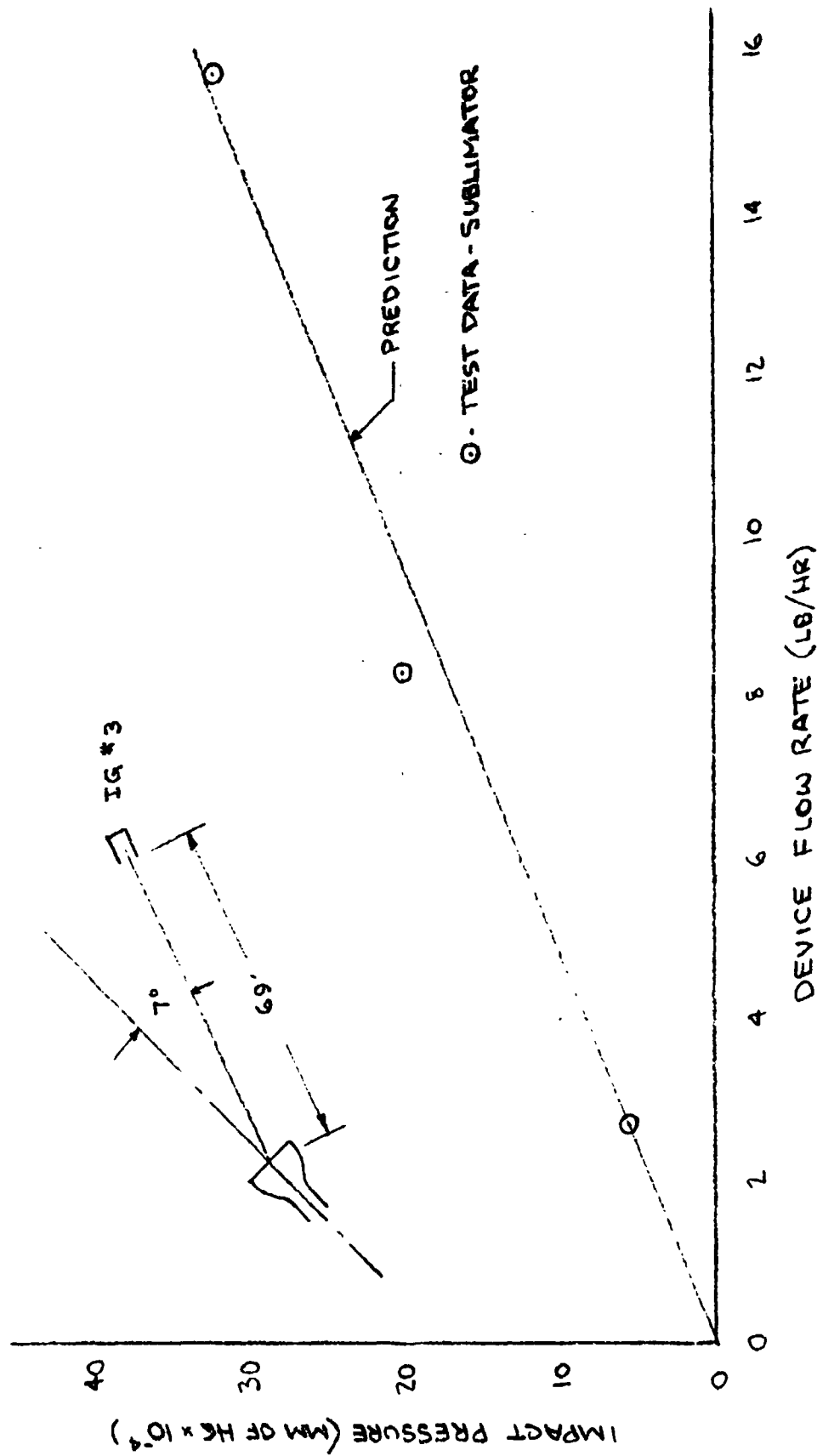


FIGURE 13
IMPACT PRESSURE DATA - SUPERSONIC NOZZLE - ION GAGE #1

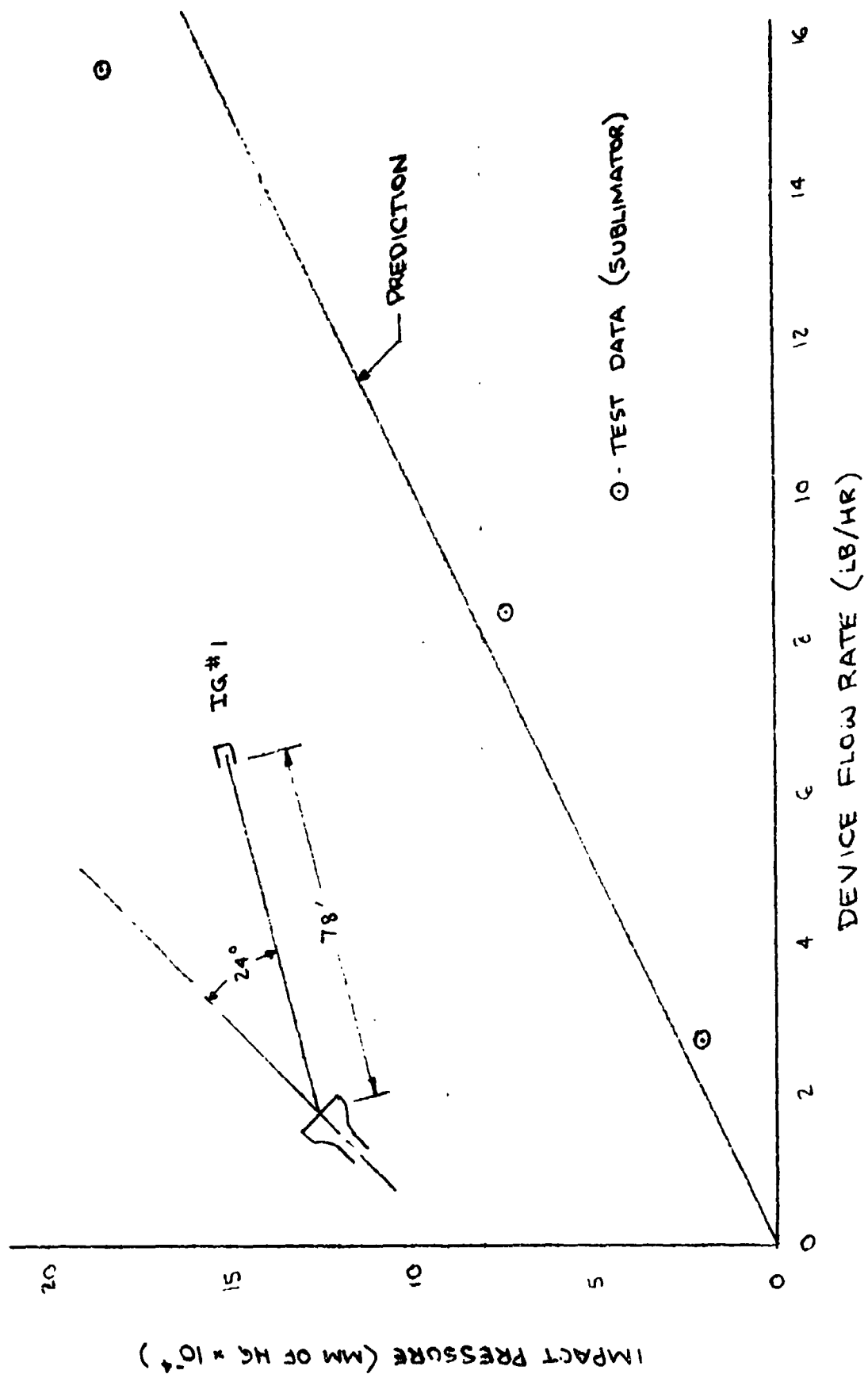


FIGURE 14
MASS FLUX DATA - SUPERSONIC NOZZLE - GCM #4

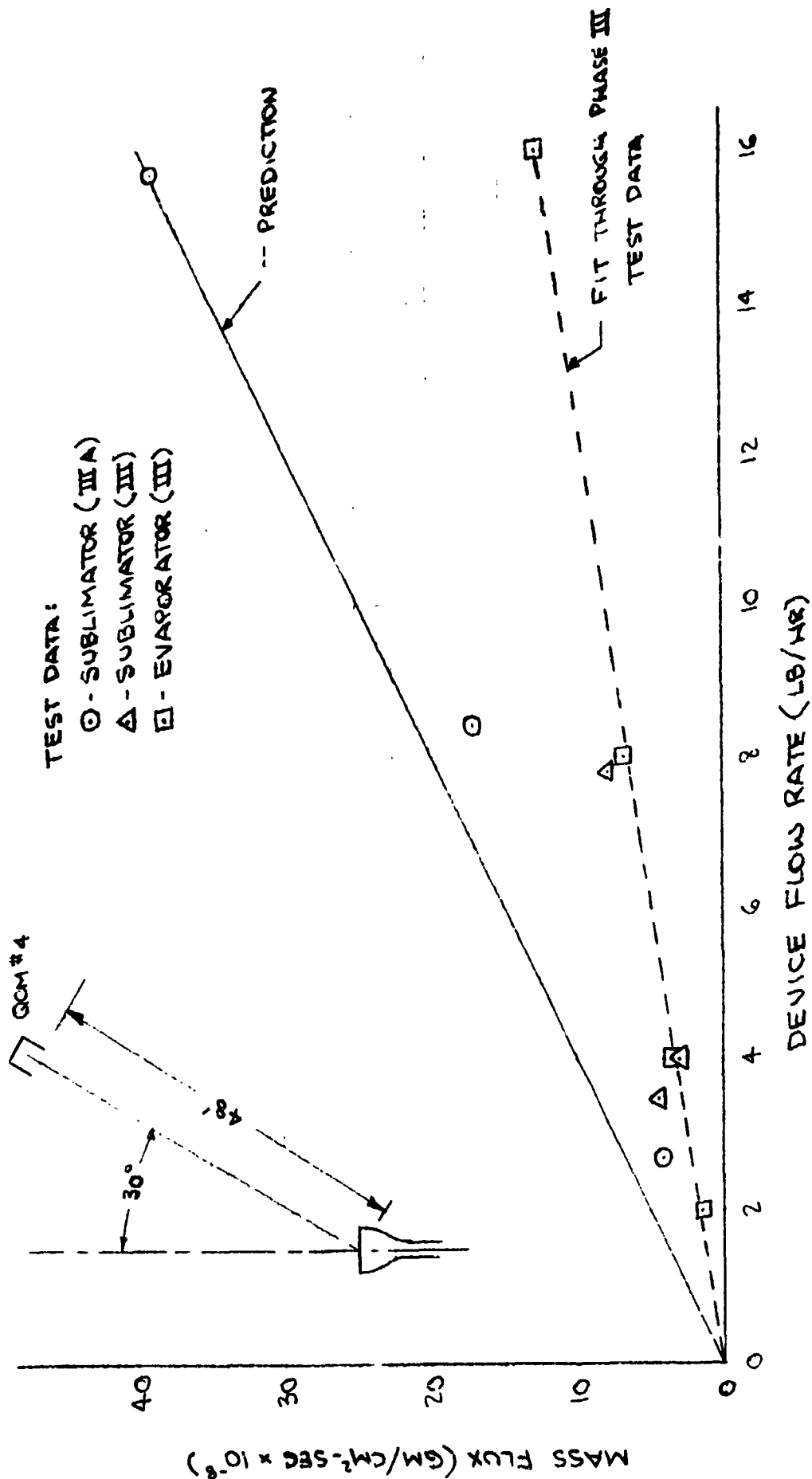


FIGURE 15
MASS FLUX DATA - NO NOZZLE - QCM # 4

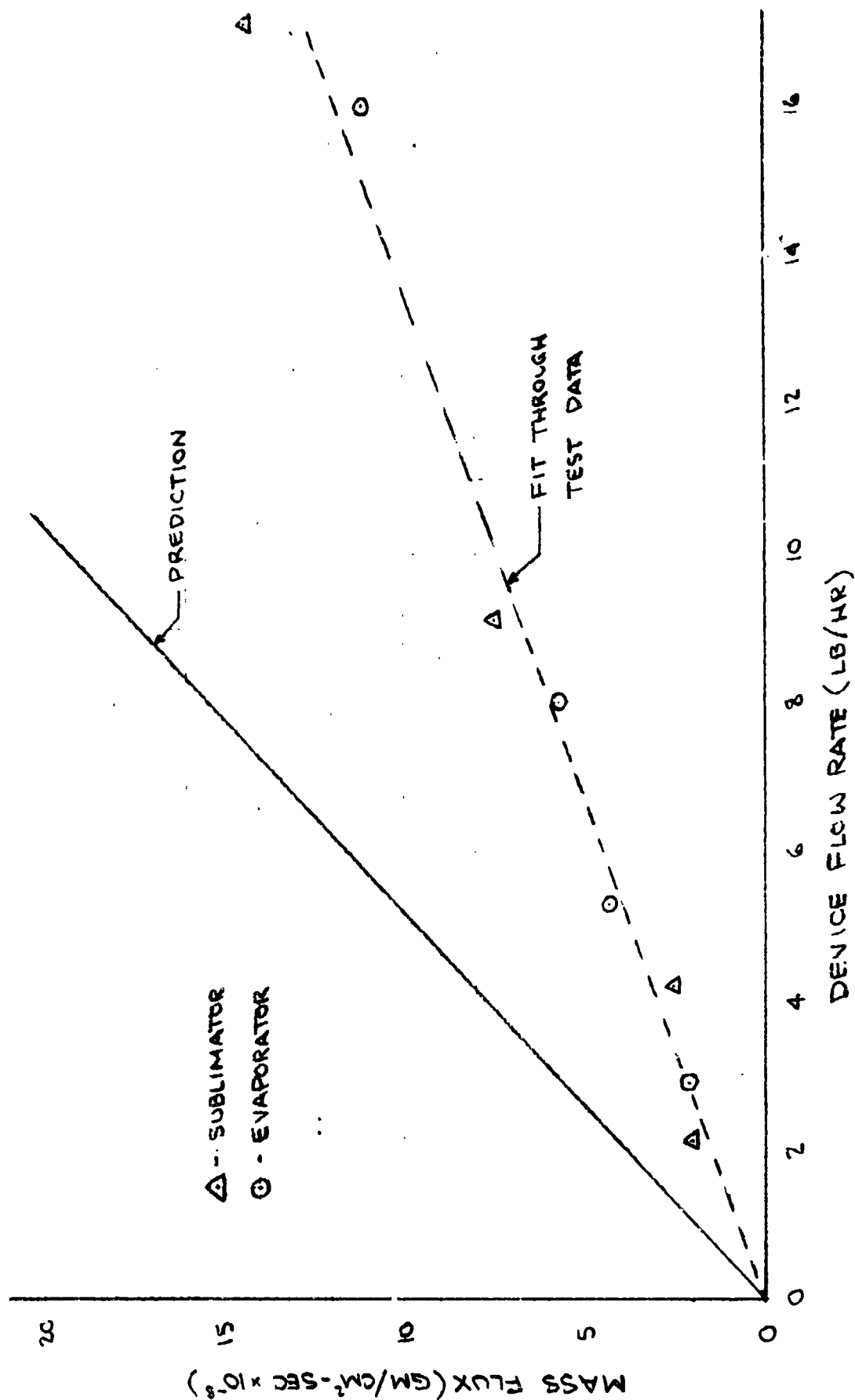


FIGURE 16
MASS FLUX DATA - PHASE III TEST - QCM # 9

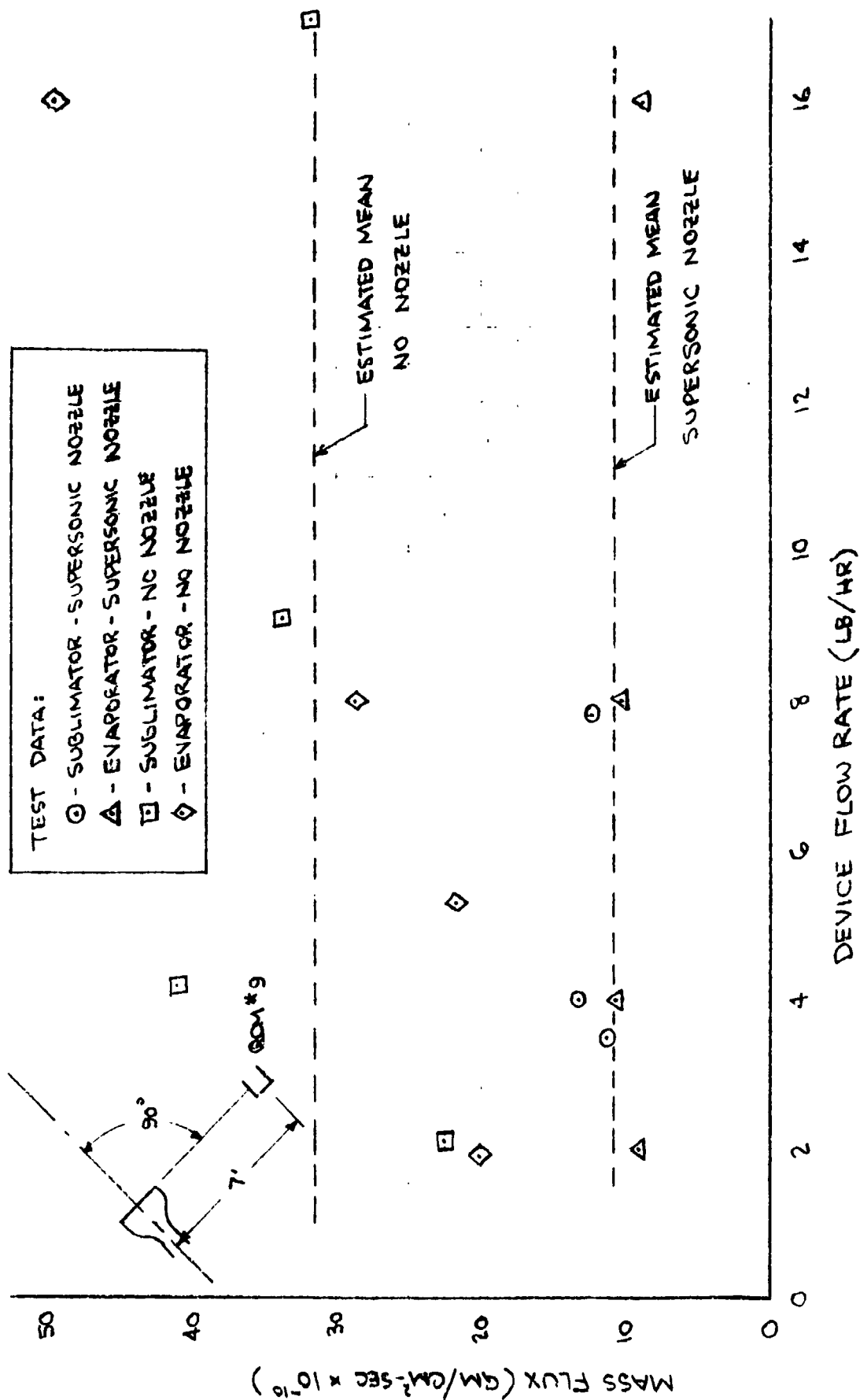


FIGURE 17

MASS FLUX DATA - PHASE III A TEST - QCM #8

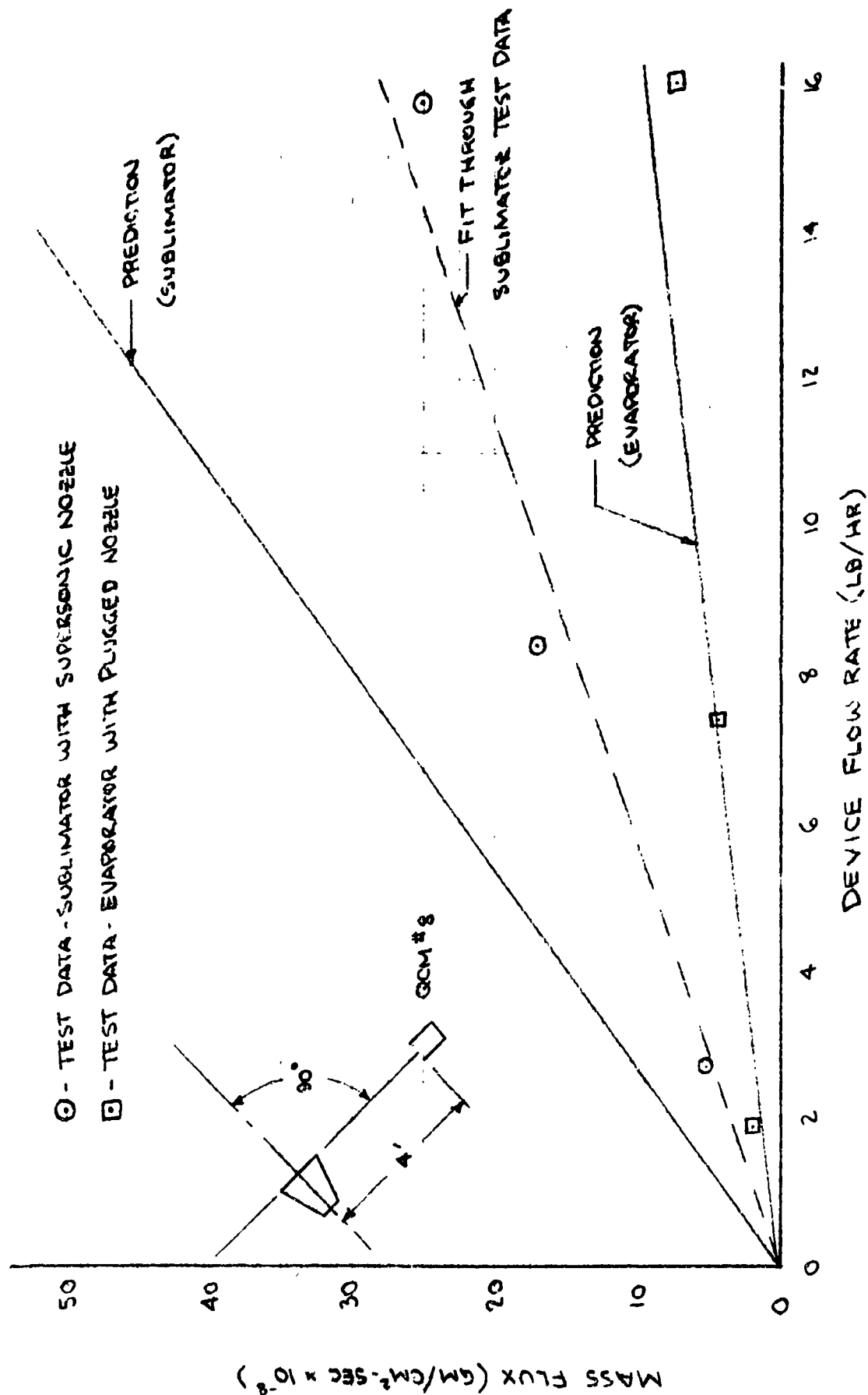


FIGURE 18
MASS FLUX DATA - PHASE IIIA TEST - QCM # 9

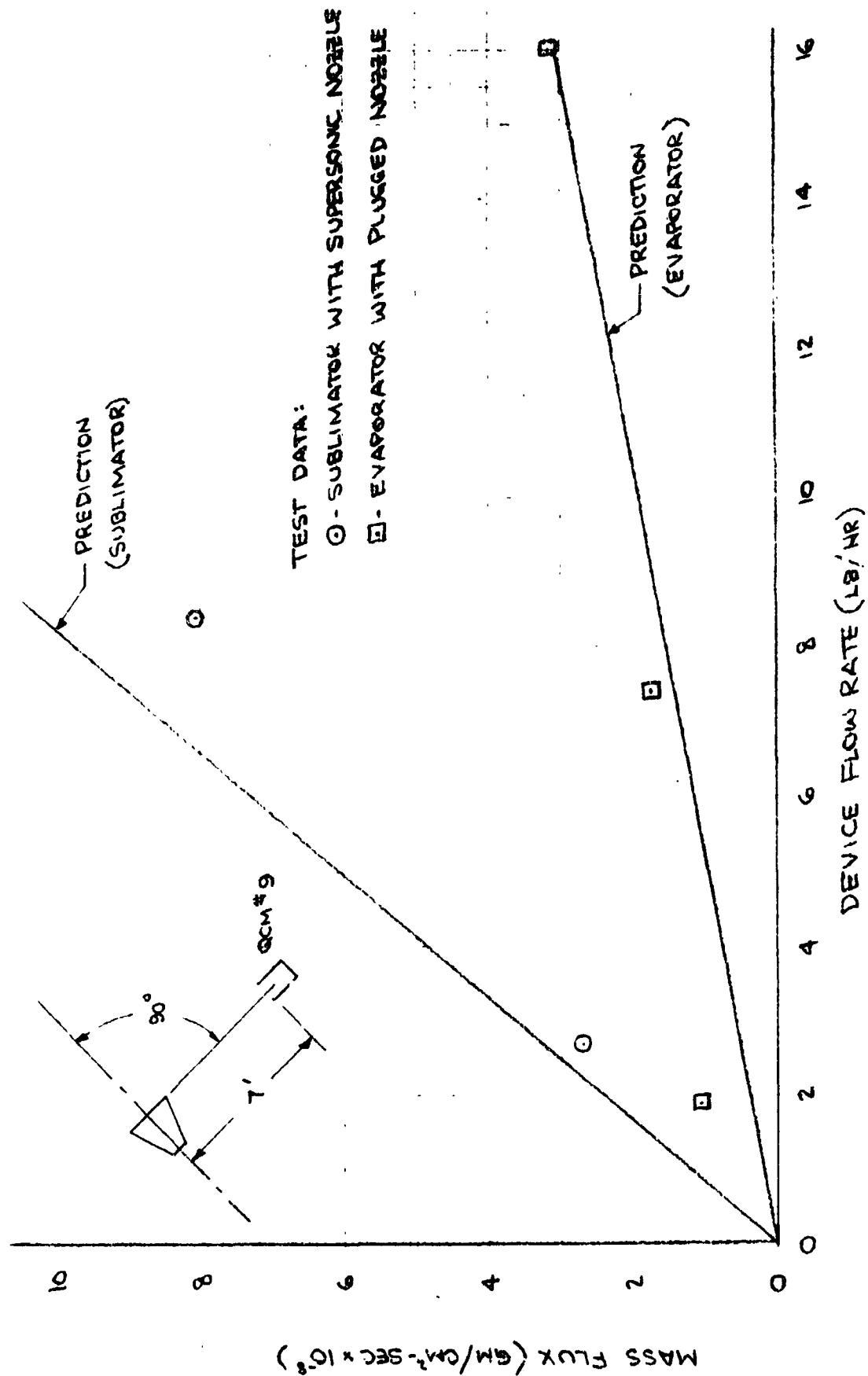
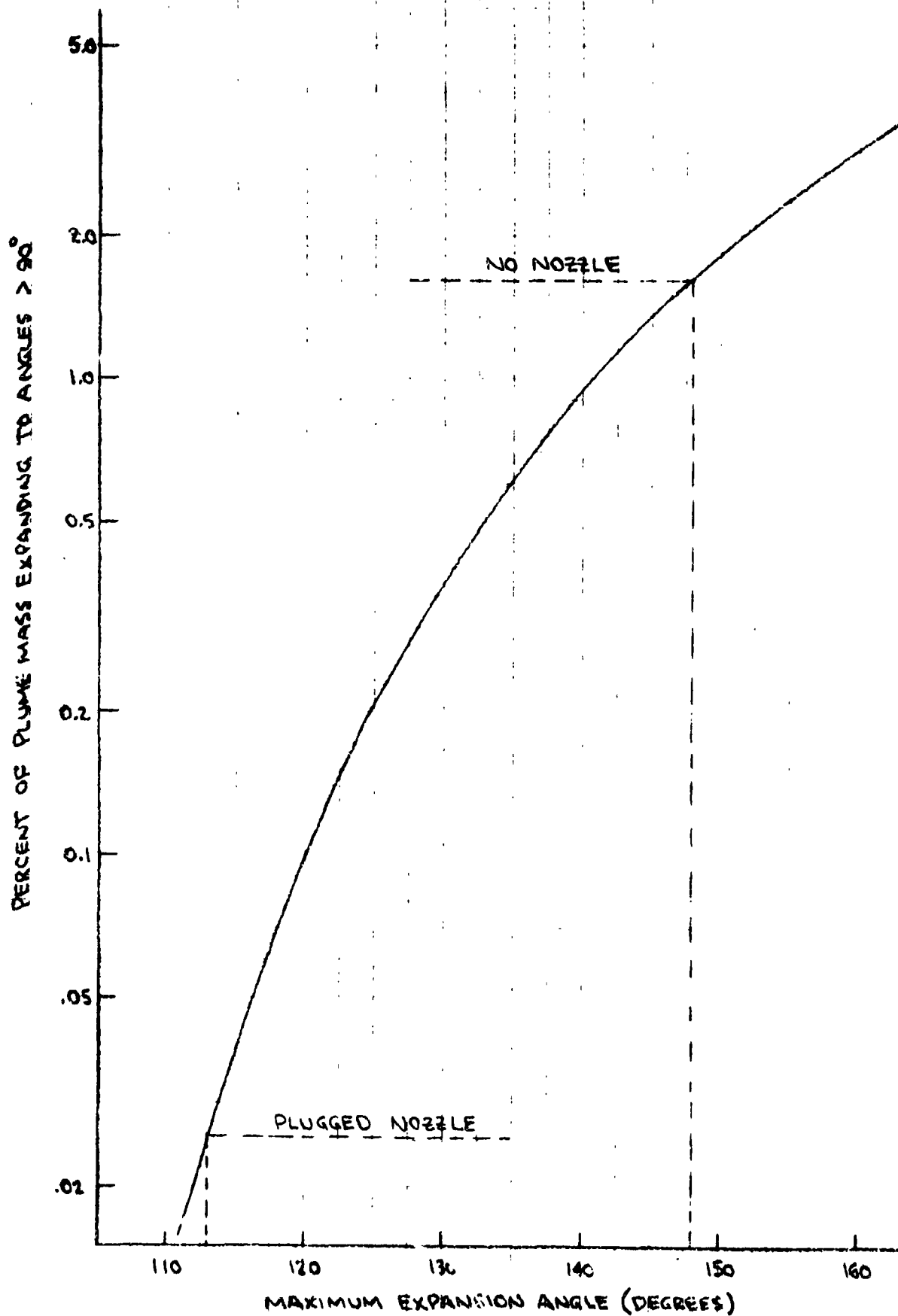


FIGURE 19
EFFECT OF EXPANSION ANGLE ON PLUME BACK FLOW



APPENDIX A

APPENDIX A
FLASH EVAPORATOR AND SUBLIMATOR
EXHAUST PLUME FLOW FIELD PREDICTIONS

Closed-form analytical expressions have been developed for both the flash evaporator and sublimator flow field properties with and without supersonic nozzles, using the techniques described in detail in Reference 2 of the body of this report. The method used is basically that of G. A. Simons, as described in the AIAA Journal, November 1972 (page 1534), which assumes modified source flow conditions and includes boundary layer effects on a conservation-of-mass basis. Reduced, working forms of the expression are summarized in this Appendix.

For the case of no nozzle, conditions correspond to expansion from a sonic orifice, and the normalized plume density field given by:

$$\frac{\rho}{\rho^*} = 0.508 \left(\frac{r^*}{r}\right)^2 \cos^6(0.608\theta) \quad (0 \leq \theta \leq 148^\circ) \quad (1)$$

where: r = radial distance from throat to point in flow field

r^* = nozzle throat radius

ρ = density at point (r, θ) in flow field

ρ^* = density at nozzle throat

θ = angular location of point in flow field relative to plume centerline

It should be noted that Equation (1) applies for both the flash evaporator and the sublimator, since both devices exhaust water vapor at essentially the same absolute total temperature. Further more, it will be noted that the absolute density (ρ) at a point in the flow field is proportional to the product $\rho^* r^{*2}$ in Equation (1). Since that product is in turn proportional to the mass flow rate of the device, it follows that

the local flow densities are the same for the two devices, for a given mass flow rate.

For the supersonic nozzle case, the flow field is represented by two expressions, one applicable to the core of the plume and the other applicable to the portion of the plume representing the expanded nozzle boundary layer. Using nozzle flow properties corresponding to the tested expansion ratio 10 configuration and assuming a laminar nozzle boundary layer development, these expressions are found to be:

Core Region

$$\frac{\rho}{\rho^*} = 1.16 \left(\frac{r^*}{r}\right)^2 \cos^6(1.01\theta) \quad (0 \leq \theta \leq 36.8^\circ) \quad (2)$$

Expanded Boundary Layer

$$\frac{\rho}{\rho^*} = 0.306 \left(\frac{r^*}{r}\right)^2 e^{-0.0773(\theta-36.8^\circ)} \quad (36.8^\circ \leq \theta \leq 148^\circ) \quad (3)$$

where the quantities are as defined for Equation (1). Again, these expressions hold for both devices, and the previous conclusion regarding equality of absolute densities is also valid. It should be noted that the expressions will give slightly low local density values for the sublimator at flow rates less than 16 lb/hr, since boundary layer properties corresponding to the 16 lb/hr flow rate were utilized. However, this effect is considered to be second order and is not present for the flash evaporator, which always generates 16 lb/hr plumes.

The plugged nozzle flow field is more complex and cannot be predicted directly by the same analytic methods. However, since the flow at the exit of the nozzle will be sonic it is assumed that the flow field will be of the same form as that from a sonic orifice or for the no nozzle configuration. It is further assumed that the design of the nozzle exit (see Figure 1) is such that the flow will be directed inward toward the centerline and

the effective maximum expansion angle of the plume will be less than that for the sonic orifice. These assumptions provide the general equation for predicting the plugged nozzle flow field, with the actual test data used to establish the effective maximum plume expansion angle. Based on a best fit of the test data the equation is:

$$\frac{\rho}{\rho^*} = 0.829(r^*/r) \cos^6(0.796\theta) \quad (0 \leq \theta \leq 113^\circ) \quad (4)$$

Given the local density, the mass flux can be readily calculated since the molecules will be moving at a velocity very near to the limiting value for expansion into a vacuum, which is 3320 ft/sec for water vapor at a stagnation temperature of 33°F. Assuming 100% capture of incident molecules, the mass flux on the QCM's is then just ρV_{MAX} . Computing this product using the above density expression, and adjusting units, the following expressions result:

Sonic Orifice (16 lb/hr)

$$\dot{m}/A \left(\frac{\text{gm}}{\text{cm}^2\text{-sec}} \right) = 0.898 \frac{\cos^6(0.608\theta)}{[r(\text{cm})]^2} \quad (0 \leq \theta \leq 146^\circ) \quad (5)$$

Supersonic Nozzle (16 lb/hr)

$$\dot{m}/A \left(\frac{\text{gm}}{\text{cm}^2\text{-sec}} \right) = 2.05 \frac{\cos^6(1.01\theta)}{[r(\text{cm})]^2} \quad (0 \leq \theta \leq 36.8^\circ) \quad (6)$$

$$\dot{m}/A \left(\frac{\text{gm}}{\text{cm}^2\text{-sec}} \right) = 0.540 \frac{e^{-.0773(\theta-36.8^\circ)}}{[r(\text{cm})]^2} \quad (36.8^\circ \leq \theta \leq 48^\circ) \quad (7)$$

Plugged Nozzle (16 lb/Hr)

$$\dot{m}/A \left(\frac{\text{gm}}{\text{cm}^2\text{-sec}} \right) = 1.465 \frac{\cos^6(0.796\theta)}{[r(\text{cm})]^2} \quad (0 \leq \theta \leq 113^\circ) \quad (8)$$

For average device flow rates other than 16 lb/hr, the mass fluxes given by these expressions must be adjusted by the ratio of the actual average flow rate to the baseline 16 lb/hr value.

Another aspect of the plume flow field is the local impact pressure prediction. For the very low density conditions of these plumes, Newtonian flow theory is applicable, and the local impact pressure is given by:

$$P_{\text{IMPACT}} = (\text{Mass Flux})(\text{Momentum Change Per Unit Mass})$$

Assuming perfect accommodation (100% capture) of the incident molecules by the Baratrons and ion gages, this expression becomes:

$$P_{\text{IMPACT}} = (\rho V)(V) = \rho V^2$$

where V is again the limiting velocity of the plume molecules, or 3320 ft/sec. Incorporating the density Equations (1), (2), (3), and (4) above into this expression and making appropriate unit conversions, the following impact pressure relationships are derived:

Sonic Orifice (16 lb/hr)

$$P_{\text{IMPACT}}(\text{mmHg}) = 68.2 \frac{\cos^6(0.608\theta)}{[r(\text{cm})]^2} \quad (0 \leq \theta \leq 148^\circ) \quad (9)$$

Supersonic Nozzle (16 lb/hr)

$$P_{\text{IMPACT}}(\text{mmHg}) = 156 \frac{\cos^6(1.01\theta)}{[r(\text{cm})]^2} \quad (0 \leq \theta \leq 36.8^\circ) \quad (10)$$

$$P_{\text{IMPACT}}(\text{mmHg}) = 47.0 \frac{e^{-.0773(\theta-36.8^\circ)}}{[r(\text{cm})]^2} \quad (36.8^\circ \leq \theta \leq 148^\circ) \quad (11)$$

Plugged Nozzle (16 lb/hr)

$$P_{\text{IMPACT}}(\text{mmHg}) = 111.25 \frac{\cos^6(0.796\theta)}{[r(\text{cm})]^2} \quad (0 \leq \theta \leq 113^\circ) \quad (12)$$

For the sublimator at mass flow rates other than 16 lb/hr, the impact pressures given by these expressions should be adjusted by the ratio of the actual mass flow rate to the 16 lb/hr value.

An important aspect of the plume flow fields for this test series is the amount of backflow, since this represents the amount of potential impingement of water vapor on the vehicle surface. This backflow can be presented in terms of fraction of the total mass flow rate which expands to angles greater than 90°F. That is:

$$R_{90} = \frac{\int_{90}^{\theta_{\max}} [\dot{m}/A] \sin \theta d\theta}{\int_0^{\theta_{\max}} [\dot{m}/A] \sin \theta d\theta}$$

where: R_{90} = fraction of flow at angles $>90^\circ$

Using the expressions for \dot{m}/A from equations (5) through (8) the values for R_{90} can be obtained analytically for each of the three configurations:

No Nozzle $R_{90} = 0.016$

Supersonic Nozzle $R_{90} = 0.00589$

Plugged Nozzle $R_{90} = 0.000257$